Aerosol and Air Quality Research, 17: 2966–2980, 2017

ISSN: 1680-8584 print / 2071-1409 online
doi: 10.4209/aaqr.2016.10.0442

The Source Apportionment of Primary $PM_{2.5}$ in an Aerosol Pollution Event over Beijing-Tianjin-Hebei Region using WRF-Chem, China

Yinglong Zhang[1], Bin Zhu[1*], Jinhui Gao[1], Hanqing Kang[1], Peng Yang[2], Lili Wang[3], Junke Zhang[3]

[1] *Key Laboratory of Meteorological Disaster, Ministry of Education (KLME), Joint International Research Laboratory of Climate and Environment Change (ILCEC), Collaborative Innovation Center on Forecast and Evaluation of Meteorological Disasters, Key Laboratory for Aerosol-Cloud-Precipitation of China Meteorological Administration, Nanjing University of Information Science & Technology, Nanjing, Jiangsu 210044, China*
[2] *Qianshan Meteorological Bureau, Anqing, Anhui 246300, China*
[3] *State Key Laboratory of Atmospheric Boundary Layer Physics and Atmospheric Chemistry (LAPC), Institute of Atmospheric Physics, Chinese Academy of Sciences, Beijing 100029, China*

ABSTRACT

The Weather Research and Forecasting model coupled to Chemistry (WRF-Chem model) was modified with an online primary $PM_{2.5}$ source-apportionment method to simulate a severe aerosol pollution episode that occurred over the Beijing-Tianjin-Hebei (BTH) region of China from October 29 to November 8, 2015. The temporal and spatial distributions and transport characteristics of this episode were examined, and the quantified primary $PM_{2.5}$ contributions by various geographical source regions to the BTH region were also analyzed in this study. The results showed that pollution in this region was mainly due to the combined effects of the synoptic conditions, terrain, and boundary layer characteristics. Before the heavy pollution event, the most parts of the BTH region were controlled by northwest wind, and the local primary $PM_{2.5}$ contribution to the BTH region accounted for 90.7%. During the heavy pollution period, the BTH region was under isobaric synoptic conditions with light horizontal winds and a stable temperature stratification structure and a lower PBLH, allowing pollutants to accumulate easily in the region. Large quantities of pollutants were transported to the BTH region from Shandong, Jiangsu, Anhui, and Henan provinces via the southerly wind, accounting for 11.6%, 9.2%, 6.7%, 11.8%, respectively. Furthermore, pollutants accumulated more significantly under a stable boundary layer structure and the northwest-southeast terrain structure. Therefore, regional contributions increased, and other polluted areas, especially the long-distance transport from a source in the Yangtze River Delta city group region, contributed about 15.9%. It should be noted that the percentage of primary $PM_{2.5}$ within the total $PM_{2.5}$ in the study period almost exceeded 50%, and in the BTH region nearly surpassed 60%. To a certain extent, primary $PM_{2.5}$ can help characterize total $PM_{2.5}$.

Keywords: WRF-Chem; Source-apportionment; Long-distance transport; Primary $PM_{2.5}$.

INTRODUCTION

In recent years, severe aerosol pollution events have occurred frequently in the Beijing-Tianjin-Hebei (BTH) region, impacting residents' health, life, and productivity (Pope *et al.*, 2003; Parrish and Zhu, 2009; Brook and Rajagopanlan, 2010; Ding *et al.*, 2013; Huang *et al.*, 2014; Zhang *et al.*, 2015). Researchers within China and around the world have investigated the distribution of aerosol concentrations and the causes of such serious pollution in this region (Okajima *et al.*, 2001; Zhao *et al.*, 2009; He *et al.*, 2011; Liu *et al.*, 2013; Li *et al.*, 2014).

Atmospheric chemistry models can be used in the quantitative analysis of regional pollution source distribution and the characterization of local pollution. Such information can be provided to the government to shape policies that reduce and control pollution. Sensitivity analysis tests are widely used to assess the roles of various pollution sources (An *et al.*, 2007; Streets *et al.*, 2007). For example, Streets *et al.* (2007) used Community Multiscale Air Quality (CMAQ) to point out that about 34% of Beijing's fine particulate matter ($PM_{2.5}$) pollution originated outside Beijing. Analytical methods developed using online aerosol source apportionment in atmospheric chemistry models can reduce calculations while providing more accurate quantitative estimates of the contribution of source regions to overall pollution levels within a target region. Li *et al.* (2008) and Wu *et al.* (2011)

* Corresponding author.
E-mail address: binzhu@nuist.edu.cn

used the Nested Air Quality Prediction Modeling System (NAQPMS) to quantify the contributions of Beijing and its surrounding areas to transportation-related pollutants within the city and determined that the surrounding regions were the greatest regional contributors to such pollution in Beijing. Long-distance transport of pollutants also significantly affects concentrations (Kevin *et al.*, 1997; Wang *et al.*, 2008; Liu *et al.*, 2010). Wang *et al.* (2014) found that pollutants traveling across the urban agglomeration of the BTH region from outside the region contributed just as much to overall pollution levels as did local pollutants, and during the period of pollution case, the influence of cross-border transport was more significant.

Aerosols in the atmosphere can be classified as primary or secondary aerosols. Primary aerosols are directly released by natural and anthropogenic emissions, while secondary aerosols are produced by chemical reactions occurred in the atmosphere. Secondary aerosols are contingent upon the presence of primary aerosols and the relevant gaseous precursors in the atmosphere. Because of this relationship and the differences of source regions and distribution of primary and secondary aerosol, the most effective way to reduce aerosol pollution is to reduce primary emissions (Fan *et al.*, 2005). In addition, some researches has also indicated that meteorological conditions and synoptic condition, including low wind speeds, a temperature inversion structure, low boundary layer height, an equalizing pressure field, and the area being behind high-pressure conditions, are the main factors of high pollutant concentrations in this area (Ji *et al.*, 2012; Wang *et al.*, 2012; Zhang *et al.*, 2013; Wang *et al.*, 2014). Moreover, the special terrain of the region surrounded on three sides by tall mountains in the BTH region is also a major contributor (Huang *et al.*, 2012; Wang *et al.*, 2014; Wu *et al.*, 2014). So far, studies on heavy pollution in the BTH region have mainly focused on the polluted area along with surrounding areas, and little research has examined the connections between two different polluted areas. In this study, the Weather Research and Forecasting model coupled to Chemistry (WRF-Chem model) was used to simulate a severe aerosol pollution episode that occurred in the BTH region in the fall of 2015. We analyzed the causes of this pollution and quantified the contributions of primary-aerosols from all the geographical sources regions in model domain by the primary $PM_{2.5}$ source apportionment method. Understanding the contributions of different source regions to pollution within the BTH will provide a valid scientific basis for conservation-oriented policies and governance of these source regions.

RESEARCH METHODS AND BASIC DATA

Model Description and Modification

The WRF-Chem model is an online mesoscale atmospheric dynamics-chemical coupling model developed by the U.S. National Oceanic and Atmospheric Administration (NOAA) and other collaborators. This model system comprises meteorological (Skamarock *et al.*, 2008) and air quality components (Grell *et al.*, 2005) with relatively comprehensive chemical and physical processes. An advantage of this model is that all physical quantities in the chemical and meteorological modules and the flux transmission scheme are fully coupled online model, which enables air quality to simulate at the same time as the meteorological model runs.

We used version 3.4 of the WRF-Chem model and developed and integrated a primary $PM_{2.5}$ tagging method into the model in order to identify the primary $PM_{2.5}$ contributions of different source regions to BTH during this episode. The tagging method is a mass-balance technique similar to particulate source apportionment technology (PSAT) that can be applied for this purpose to any region (Ying and Kleeman, 2006; Wagstrom *et al.*, 2008). It tracked and calculated the concentrations of $PM_{2.5}$ originating in different source regions (the independent variable) within the larger simulated region. The tracers in this tagging method account for the effects of physical processes (e.g., advection, vertical mixing, convection), as the normal simulation does, but do not disrupt the normal calculations. This case study was limited in that we only tagged primary $PM_{2.5}$ pollution, and the $PM_{2.5}$ source-apportionment is not complete, the secondary aerosols were not included.

In this method, the simulation domain was divided into 17 source regions (Fig. 1(a)). And the primary $PM_{2.5}$ identified with each source region was tracked as an independent variable. For each time step, the concentration of primary $PM_{2.5}$ with identification by i is determined using the following equation:

$$C_i(t + \Delta t) = C_i(t) + \Delta C_i \quad (1)$$

where $C_i(t)$ is the primary $PM_{2.5}$ concentration with identification of i at the time of t, Δt is the time step, ΔC_i is the change in concentration of primary $PM_{2.5}$ at this time step. ΔC_i is determined by the following equation:

$$\Delta C_i = \Delta Chem_i + \Delta Phy_i + \Delta Emis_i \quad (2)$$

where $\Delta Chem_i$ is the concentration changes caused by chemical reactions. In aerosol chemistry, primary $PM_{2.5}$ doesn't participate in the chemical calculation which means the $\Delta Chem_i$ is 0. ΔPhy_i is the sum of the physical processes (including advection, vertical mixing, dry and wet deposition, and convection). Each tracked variable undertakes all the relevant calculations of the physical processes as the normal simulation do, but does not perturb the normal model calculations, so the concentration changes caused by physical processes will be obtained directly.

$\Delta Emis_i$ is the gross emission production within region i, determined by:

$$\Delta Emis_i(\mathrm{x},\mathrm{y},\mathrm{z}) = \begin{cases} \Delta Emis(\mathrm{x},\mathrm{y},\mathrm{z}) & :inside\ region\ i \\ 0 & :outside\ region\ i \end{cases} \quad (3)$$

For any grid in domain, if it is in the region i, then the $\Delta Emis_i(x, y, z)$ equals $\Delta Emis(x, y, z)$, otherwise, it equals zero.

Compared with classic sensitivity analysis, this primary $PM_{2.5}$-tagging model provides a more accurate measurement of primary $PM_{2.5}$ concentrations in all related regions, while

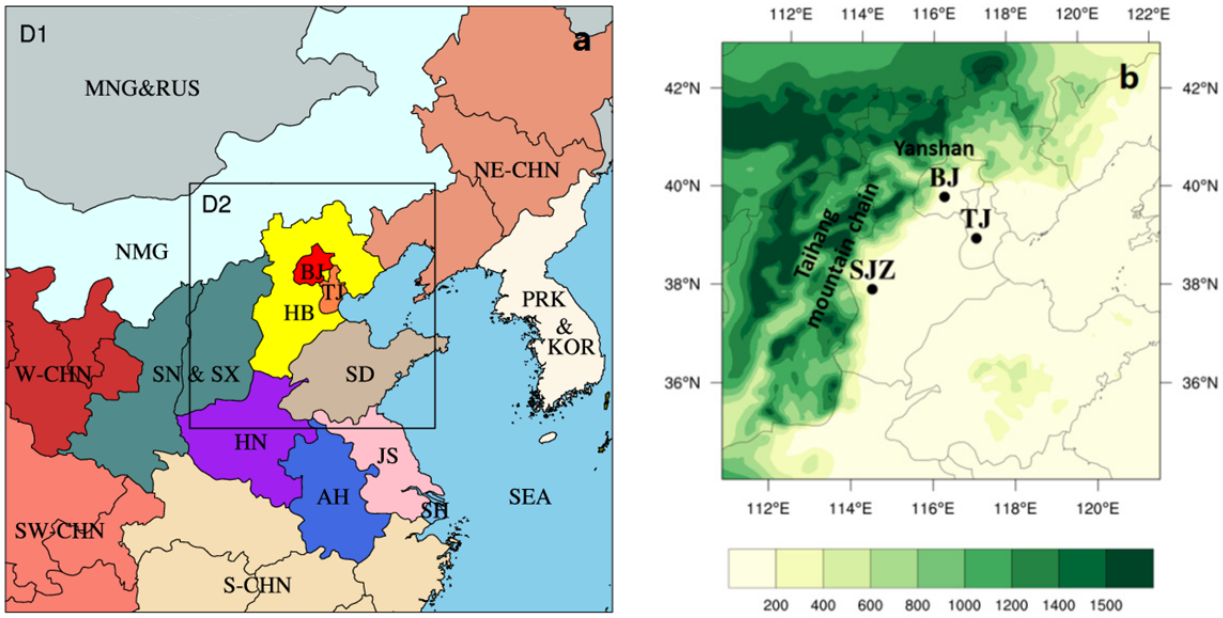

Fig. 1. a) Nested domains and regional divisions, b) terrain height in simulation area, domain 2.

reducing calculation errors (Li *et al.*, 2008). The primary $PM_{2.5}$-tagging by source regions method can also be applied to other pollutants. For example, Gao *et al.* (2016) used this method to analyze ozone sources over the Yangtze River Delta.

Model Settings and Basic Data

Fig. 1(a) shows the model domains, which included two nested domains on a lambert projection with horizontal resolutions of 36 and 12 km and grids of 90 × 90 and 108 × 108, respectively. The parent domain, D1, supported reasonable meteorological and chemical boundary conditions for the nest domain, D2. Vertically, there were 27 sigma levels between the surface pressure and 50 hPa. The simulation was conducted between 08:00 on October 27, 2015 Local Standard Time (LST) and 08:00 on November 8, 2015 (LST), and the first two days were used as the spin-up time. The carbon-bond mechanism Z (CBM-Z) (Zaveri and Peters, 1999), a gas-phase physical mechanism based on CBM-IV and containing 134 reactions for 55 species, and MOSAIC (4 bins) (Zaveri *et al.*, 2008) aerosol chemistry (divided into four aerosol bins: 0.039–0.156 μm, 0.156–0.625 μm, 0.625–2.5 μm, and 2.5–10 μm) were applied to the WRF-Chem model. The remaining model parameter options are shown in Table 1.

The initial and boundary meteorological conditions for WRF-Chem were taken from the U.S. National Centers for Environmental Prediction (NCEP) Final (FNL) Operational Global Analysis data files with 1° × 1° horizontal resolution at 6-h intervals. The anthropogenic emission inventory used in this case study was the Multi-resolution Emission Inventory for China (MEIC) 2012 with a horizontal resolution of 0.25° × 0.25°. Observational data for model evaluation were used from eight cities: Beijing (BJ), Tianjin (TJ), Shijiazhuang (SJZ), Zhangjiakou (ZJK), Shandong (SD), Jiangsu (JS), Anhui (AH), and Henan (HN). Data included meteorological elements (sea-level pressure, temperature, wind speed, and wind direction) and $PM_{2.5}$ concentrations. The detail description and location of each region were showed in Table 2 and Fig. 1(a). In this case study, the model domain was divided into 17 source regions (shown in Fig. 1(a)): 1) Beijing, 2) Tianjin, 3) Hebei, 4) Shandong, 5) Shanxi and Shaanxi, 6) Inner Mongolia, 7) NE-CHN (Heilongjiang, Jilin, and Liaoning), 8) Henan, 9) Anhui, 10) Jiangsu, 11) Shanghai, 12) W-CHN (Qinghai, Gansu, and Ningxia), 13) SW-CHN (Yunnan, Guizhou, Sichuan, and Chongqing), 14) S-CHN (Hubei, Hunan, Jiangxi, Fujian, and Zhejiang), 15) Russia and Mongolia, 16) Korean Peninsula, and 17) sea.

Table 1. Physical parameters used in the modeling study.

Item	Selection	Reference
Microphysics scheme	Lin *et al.* scheme	Lin *et al.* (1983)
Short-wave radiation option	Goddard short scheme	Chou and Suarez (1994)
Long-wave radiation option	RRTM scheme	Mlawer *et al.* (1997)
Cumulus physics option	Grell 3D ensemble scheme	Grell (1993)
Photolysis option	Fast-J photolysis	Wild *et al.* (2000)
Land surface option	Noah land-surface model	Chen and Dudhia (2001)
Boundary layer option	YSU scheme	Hong *et al.* (2006)
Dry deposition	Wesely	Wesely (1989)

Table 2. Tagged primary $PM_{2.5}$ production regions in Fig. 1(a).

Region	Description
BJ	Beijing, China
TJ	Tianjin, China
HB	Heibei province, China
BTH	Beijing, Tianjin, Hebei
S-HB	Southern Hebei, including Shijiazhuang, Xingtai, Handan, Hengshui, Cangzhou, Baoding, and Langfang
N-HB	Nouthern Hebei, including Zhangjiakou, Tangshan, Chengde and Qinhuangdao
SJZ	Shijiazhuang, Hebei
ZJK	Zhangjiakou, Hebei
NE-CHN	Northeast China, including Heilongjiang, Jilin and Liaoning provinces, China
S-CHN	South China, including Hubei, Hunan, Jiangxi, Fujian and Zhejiang provinces, China
SW-CHN	Southwest China, including Yunnan, Guizhou, Sichuan and Chongqing provinces, China
W-CHN	West China, including Qinghai, Gansu and Ningxia provinces, China
JS	Jiangsu province, China
AH	Anhui province, China
HN	Henan province, China
SD	Shandong province, China
SN & SX	Shaanxi province & Shanxi province, China
MNG	Mongolia
NMG	Inner Mongolia province, China
RUS	Russia
PRK & KOR	Democratic People's Republic of Korea & Republic of Korea

MODEL EVALUATION

The observed and simulated meteorological data on sea-level pressure (SLP), temperature (T), wind speed (Wspd), and wind direction (Wdir) and the $PM_{2.5}$ data from these four cities and eight cities are shown in Figs. 2 and 3, respectively, and all cities statistical results are summarized in Table 3. The Mean Bias (MB), Normalized Mean Bias (NMB), Normalized Mean Error (NME), the Root-Mean-Square Error (RMSE), and correlation coefficient (r) are displayed. We found that the WRF-Chem model accurately simulated trends and peak distribution, as well as the $PM_{2.5}$ levels at all stations except SJZ. As shown in Table 3, the correlation coefficient *r* of Wspd was low (0.46), and RMSE was too high (131.62) at SJZ. Possible causes of these faulty simulations are stronger and higher uncertainty of emission sources, and worse capability in simulation of wind direction and wind speed (in Fig. 2(k)) under complex terrain around SJZ.

Fig. 3 shows that the model successfully reproduced $PM_{2.5}$ concentrations during this period. From these $PM_{2.5}$ levels, we can see that severe pollution was present on November 3 and 5, with the most serious pollution ($PM_{2.5}$ concentration exceeding 300 μg m^{-3}) in the region appearing at around 00:00 (LST) on November 5. Based on the $PM_{2.5}$ concentration levels and evolution in the BTH region, we divided the pollution process into four stages: stage 1, from October 29 to 30; stage 2, from October 31 to 12:00 LST on November 2; stage 3, from November 3 to 06:00 LST on November 5; and stage 4, from 12:00 LST on November 5 to 12:00 LST on November 7, representing clean, light, heavy, and then clean pollution periods, respectively (We discuss this in more detail in the following part.).

ANALYSIS AND DISCUSSION

Description of Synoptic Conditions and Simulated $PM_{2.5}$ Distributions

Meng and Cheng (2002) pointed out that pollutants can accumulate in light horizontal winds on the local scale more easily when Beijing is under uniform pressure type of surface synoptic conditions. The condition of Beijing in front of high-pressure systems has been found to facilitate the spread of pollutants (Miao *et al.*, 2015). Fig. 4 presents surface synoptic conditions, which varied throughout the study period. The wind was blowing northwest when the BTH region was under high-pressure conditions at 02:00 LST on October 30 showed in Fig. 4(a). This high pressure then weakened near the central region of Mongolia, but another high pressures then covered a wide area of southeastern China, leading to a weak pressure gradient and low wind speeds in the BTH region at 02:00 LST on November 2 presented in Fig. 4(b). In Fig. 4(c), the BTH region was in saddle field with low wind speeds at 02:00 on November 4. Finally, strong high-pressure conditions near Mongolia and Inner Mongolia and low pressures in southern China led to a dense pressure gradient and gale at 02:00 LST on November 6 in Fig. 4(d).

Figs. 5(a)–5(d) show the average spatial distribution of surface $PM_{2.5}$ and wind fields during the four different stages. From Figs. 5 and Fig. 1(b), we can see that the terrain of the Taihang Mountains (northeast-southwest) and Yanshan Mountain (east-west) served as important demarcation lines for wind conditions and pollution concentrations. The altitude of most of the Taihang Mountains is over 1,200 m, and that of the Yanshan Mountains ranges between 600 and 1,500 m. Thus, this special terrain exerts a significant effect on the BTH region. The terrain weakens the north winds,

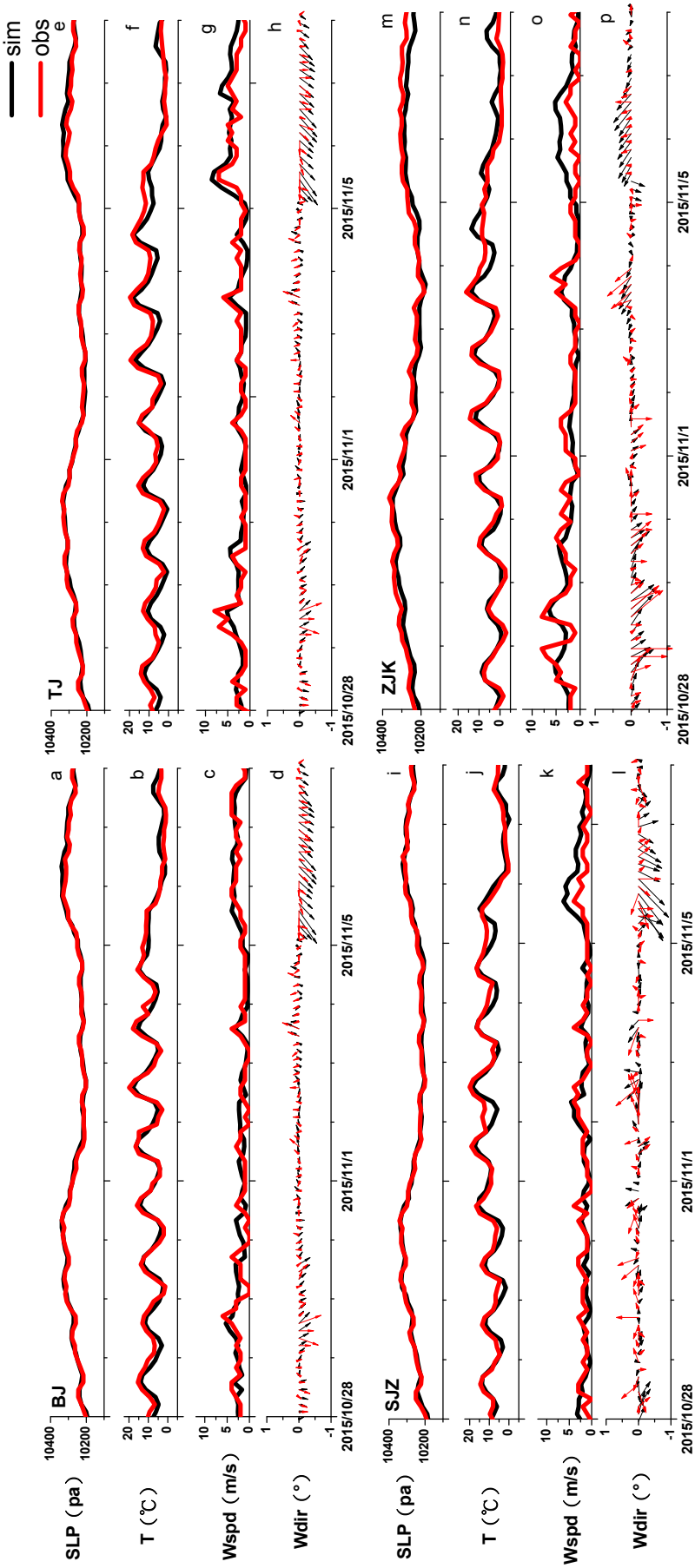

Fig. 2. Comparison between observed (red) and simulated (black) meteorological parameters in four representative cities of BTH region.

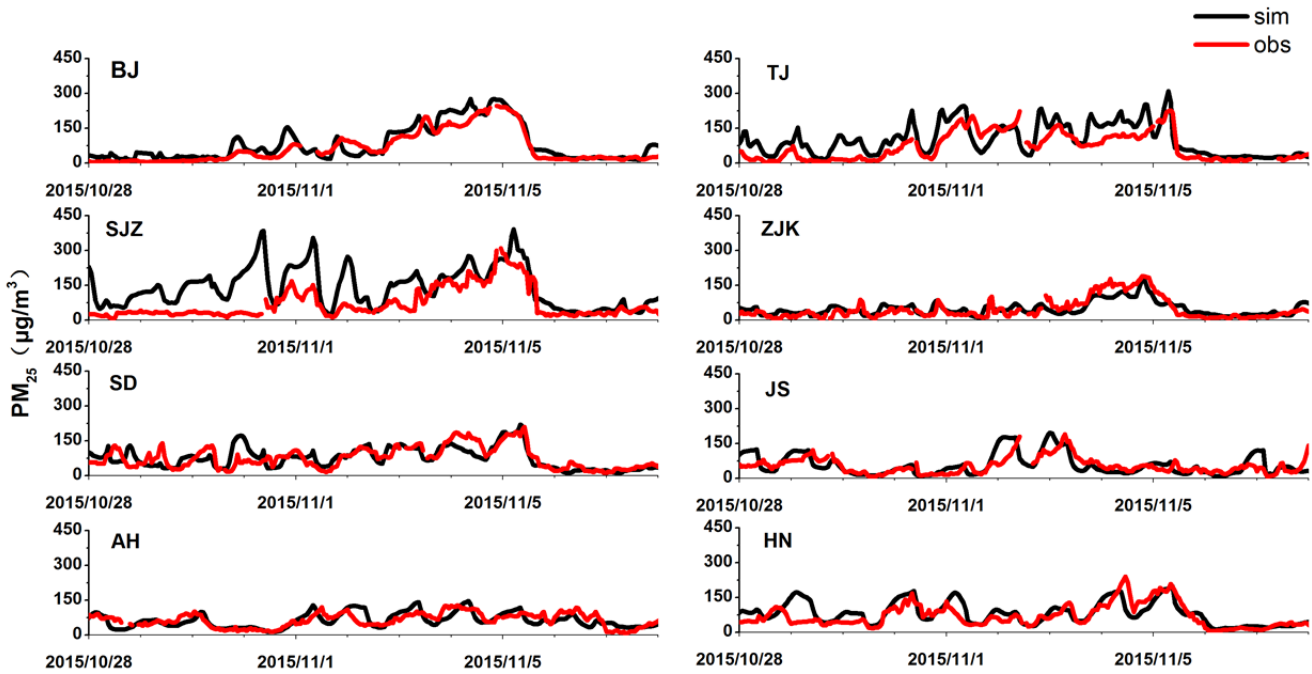

Fig. 3. Comparison between observed (red) and simulated (black) daily average $PM_{2.5}$ concentrations in eight representative cities.

while contaminants easily accumulate at the foot of the mountain under the control of southerly wind (Miao *et al.*, 2015).

During stage 1 (Fig. 5(a)), the northern BTH region was experiencing a northwest gale, which improved air quality. The pollutants at the foot of the two mountains in the BTH region could not be eliminated completely. However, owing to low wind speeds in southern BTH region, the average $PM_{2.5}$ concentration in this region was almost under 60 μg m^{-3}, within Grade II of the Chinese National Ambient Air Quality Standards. In stage 2 (Fig. 5(b)), when the wind in the south turned southwest wind, light levels of pollutants were beneficial to transport into the BTH region. Moreover, the mountainous terrain weakened the speed of the north wind, which in turn aggravated pollution levels at the foot of the mountain and formed a pollution zone from southwest to northeast (including in Shijiazhuang, Baoding, and Tianjing), similar to findings by Wu *et al.* (2014) and Ren *et al.* (2004). It is worth noting that northwestern BJ was still in a clean state owing to greater wind speeds in the North. Shortly afterwards, North China was dominated by southerly winds and wind in south region greater than before (stage 3, Fig. 5(c)), which facilitated the long-distance transport of pollutants from the southern regions. The wind speed over BJ and TJ was low, which allowed pollutants to accumulate after being transported to these areas. Furthermore, BJ was not protected by the northwest wind as the wind shifted south in the northern mountains, and a high level of pollution moved into BJ. The maximum observation concentration of $PM_{2.5}$ was 304 μg m^{-3}, occurring at 20:00 LST on October 4 in BJ. This was also the point at which $PM_{2.5}$ reached its widest scope and largest concentration in such a special terrain structure. Finally, when the wind over most of North China shifted northeast (stage 4, Fig. 5(d)), fresh air was driven into the BTH region, and $PM_{2.5}$ concentrations decreased quickly to below 40 μg m^{-3}, within Grade I of the Chinese National Ambient Air Quality Standards.

Primary $PM_{2.5}$ Contributions of Different Geographical Source Regions to the BTH Region

Pollution source apportionment is an effective method of studying the source regions of air pollutants. Fig. 6(a) illustrates the primary $PM_{2.5}$ contributions of different geographical source regions to the BTH region. Fig. 6(b) presents the average spatial distribution of the primary-to-total $PM_{2.5}$ ratio within the study period. We can see that the percentage of primary $PM_{2.5}$ almost exceeds 50% in most of domain 1 and nearly surpasses 60% in the BTH region. Because the high ratio of primary $PM_{2.5}$ and the precursors of secondary $PM_{2.5}$ close related to primary $PM_{2.5}$ in source regions, further source apportionment of primary $PM_{2.5}$ will help characterize total $PM_{2.5}$. As seen in Fig. 6(a), in stage 1, primary $PM_{2.5}$ originated mainly in the local region. The wind on the northern mountains was stronger than the southern. The upstream region with clean air had almost no primary $PM_{2.5}$ contribution to the downstream region. In stage 2, when the wind speed become small on the northern side of the two mountains and wind shifted southwest on the southern side, a light pollution zone at the foot of the mountains from SJZ to TJ was created by both wind fields and the terrain. Moreover, northwestern BJ is clean due to it was still experiencing northwest winds, so only southeastern BJ occurred light air pollution. Fig. 7 shows the average primary $PM_{2.5}$ contributions to the BTH region by several geographical source regions. We can clearly

Table 3. Comparisons of statistical parameters between simulated and observed variables in eight representative cities of BTH region (Unit: $PM_{2.5}$ (μg m^{-3}); P (pa); T (°C); Wspd (m s^{-1}); Wdir (°)).

Sites	Var	*r*	MB	NMB (%)	NME (%)	RMSE
BJ	$PM_{2.5}$	0.93	8.15	14.78	37.00	23.21
	P	0.99	3.59	0.03	0.07	8.64
	T	0.95	–0.29	–3.50	18.08	1.76
	Wspd	0.55	0.24	12.75	50.12	1.17
	Wdir	0.74	7.53	4.81	25.23	57.68
TJ	$PM_{2.5}$	0.74	30.79	43.10	62.21	64.42
	P	0.96	2.47	0.02	0.08	11.19
	T	0.94	–1.55	–17.80	22.67	2.27
	Wspd	0.70	0.78	29.92	58.43	2.03
	Wdir	0.73	30.36	18.02	26.47	56.44
SJZ	$PM_{2.5}$	0.63	66.65	88.86	94.68	131.62
	P	0.98	–2.20	–0.02	0.07	8.12
	T	0.92	–1.33	–13.68	19.07	2.33
	Wspd	0.46	0.23	14.48	60.05	1.27
	Wdir	0.67	20.45	10.21	29.75	84.15
ZJK	$PM_{2.5}$	0.65	–3.47	–6.71	41.06	14.83
	P	0.97	–18.73	–0.18	0.18	21.57
	T	0.90	0.47	11.16	42.74	2.20
	Wspd	0.52	0.30	14.73	61.83	1.56
	Wdir	0.83	–14.65	–6.85	25.36	71.16
SD	$PM_{2.5}$	0.70	1.13	1.38	36.48	46.79
	P	0.97	–4.17	–0.04	0.07	9.89
	T	0.79	–1.00	–9.27	23.64	3.02
	Wspd	0.51	1.91	77.85	89.16	2.71
	Wdir	0.79	–5.26	–4.68	27.31	39.67
JS	$PM_{2.5}$	0.52	0.33	0.58	47.50	38.58
	P	0.98	–0.40	0.00	0.06	8.05
	T	0.92	0.74	5.02	11.80	2.03
	Wspd	0.67	0.97	38.89	54.21	1.71
	Wdir	0.87	–2.14	–1.13	18.15	52.50
AH	$PM_{2.5}$	0.64	–1.71	–2.65	33.13	23.48
	P	0.98	–8.13	–0.08	0.09	11.38
	T	0.83	1.27	8.67	14.64	2.78
	Wspd	0.66	1.21	58.43	71.52	1.77
	Wdir	0.87	18.30	13.08	23.34	44.87
HN	$PM_{2.5}$	0.59	3.08	3.68	43.03	46.31
	P	0.98	–2.98	–0.03	0.07	8.84
	T	0.88	0.04	0.36	17.35	2.40
	Wspd	0.57	1.20	49.11	60.07	1.82
	Wdir	0.93	0.56	0.48	18.69	34.98

see that BJ was mostly affected by primary $PM_{2.5}$ originating locally and from HB, accounting for 68.7% and 23.4%, respectively, of total primary $PM_{2.5}$ contributions. In TJ, primary $PM_{2.5}$ originated mainly in TJ itself and HB, accounting for 31.2% and 54.2% of the total, respectively. The primary $PM_{2.5}$ in HB was mainly from HB itself, accounting for 69.4% of the total. So we can know that the local contribution of $PM_{2.5}$ to the BTH region accounted for 90.7% of total primary $PM_{2.5}$ before the heavy pollution event (stage 1 and stage 2), and HB, TJ, and BJ made up 53.6%, 21.0%, and 16.1%, respectively.

In stage 3, when the wind in the northern mountains shifted southerly, pollutant concentrations rapidly increased in BJ. Southwest winds shifted south, and a gale weakened into soft winds in the middle of the BTH region, which allowing for greater concentrations and a wider range of pollution. In this stage, BJ, TJ, and HB were most affected by the regions also shown in Fig. 7. BJ and HB were the regions that most significantly contributed to primary $PM_{2.5}$ in BJ, accounting for 25.0% and 26.7% of the total primary $PM_{2.5}$, respectively. Pollution in TJ was contributed primarily by TJ itself, as well as HB and SD, accounting for 30.5%, 20.9%, and 15.0% of the total, respectively. HB was mainly affected by pollution from HB, HN, and SD, accounting for 38.2%, 16.9%, and 10.2% of the total, respectively. So the BTH region contributions by BTH, Shandong, Henan, Jiangsu and Anhui accounted for 50.7%, 11.6%, 11.8%, 9.2% and 6.7%, respectively. AH, JS, SD and HN all had an obvious

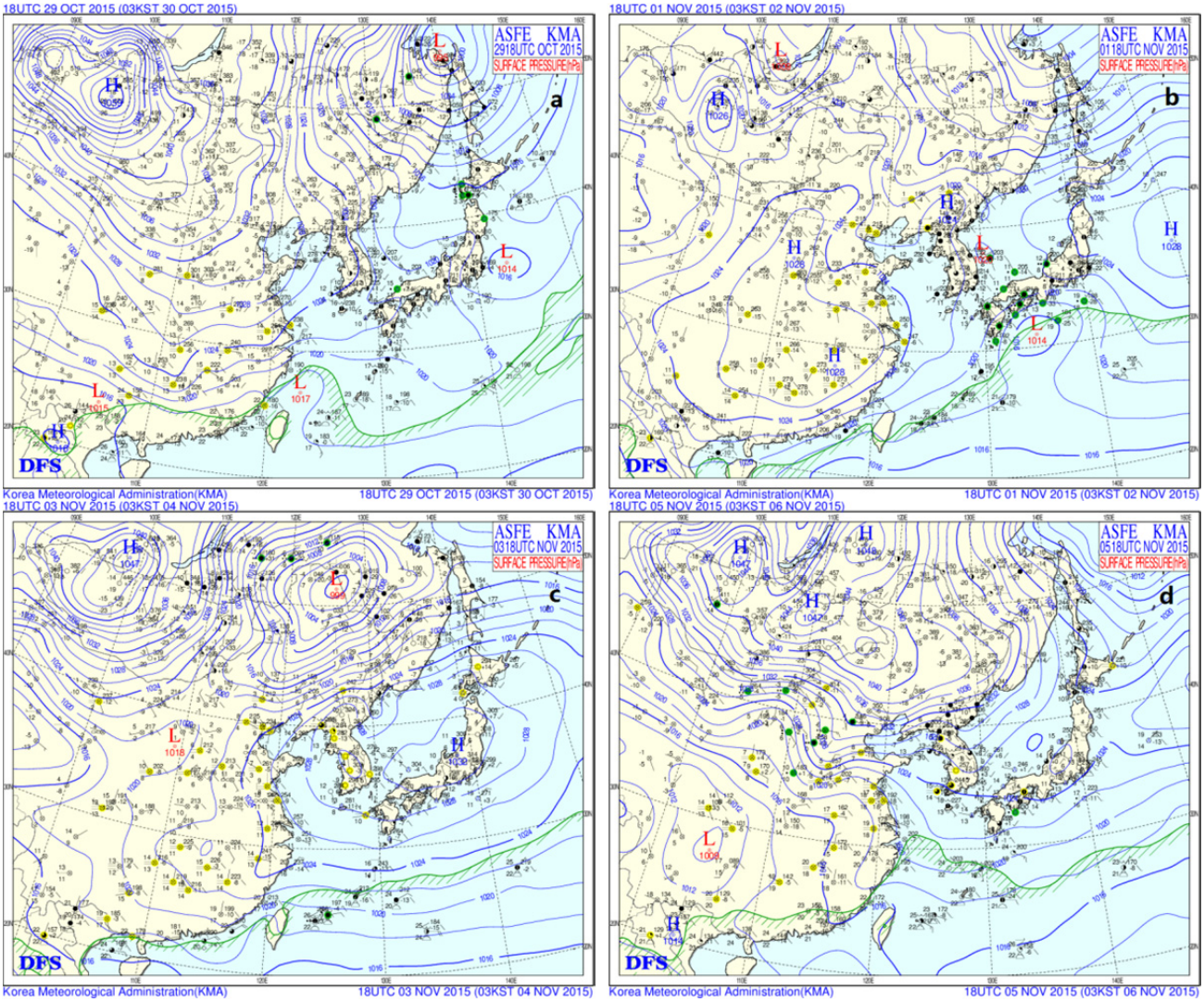

Fig. 4. Maps of surface synoptic conditions at 02:00 LST on a) Oct. 30, b) Nov. 2, c) Nov. 4, and d) Nov. 6, respectively.

effect on the BTH region, and the primary $PM_{2.5}$ concentration contribution in S-HB (Shijiazhuang, Xingtai, Handan, Hengshui, Cangzhou, Baoding, and Langfang) was greater than in N-HB (Zhangjiakou, Tangshan, Chengde and Qinhuangdao). Finally, pollution in the BTH region cleared out quickly owing to the shifting of the northeast gale in stage 4.

Through all the study period, by combining the pollution processes with the synoptic conditions map, we determined that the pollution phenomenon began with the appearance of high-pressure conditions in southern China and decreasing high-pressure in northern China in stage 2, while an isobaric synoptic condition in the BTH region led to the most severe pollution and long-distance transport of pollutants from JS, AH, and HN to the BTH region in stage 3. So we will discuss stage 3 in detail to reveal the reason of the severe pollution.

Long-Distance Transport during Heavy Pollution Periods in Stage 3

PBL Characteristics

Lyu *et al.* (2012) indicated that Planetary Boundary Layer Height (PBLH) determines the efficiency of pollutant diffusion. Higher PBLH is beneficial to pollutant diffusion, while lower PBLH allows pollution to accumulate in the boundary layer (Guo *et al.*, 2011; Yang *et al.*, 2011; Ye *et al.*, 2011). As shown in Fig. 8, only 200 m of the PBLH and horizontal distribution of wind divergence were drew in stage 3, we can see that the PBLH of BJ and SJZ was below 200 m. Compared Fig. 5(c) with Fig. 8, which reveal high $PM_{2.5}$ concentrations correspond to low PBLH. And we also can clearly see a large wind convergence region (the parallelogram area in Fig. 8) caused by high wind speed in the south and low speed in the region of the southwest-northeast direction (from BJ to SJZ). Therefore $PM_{2.5}$ pollutants easily accumulated in this parallelogram area, which is similar to the study by Yang *et al.* (2016).

To help characterize the vertical structure, we used the profiles shown in Figs. 9(a) and 9(b) (from the black straight lines in Fig. 8). Fig. 9(a) (from the black southeast-northwest straight line in Fig. 8, including BJ and TJ) reveals that pollutants were continuously transported to the BTH region by the southerly wind, but the tall mountains blocked their

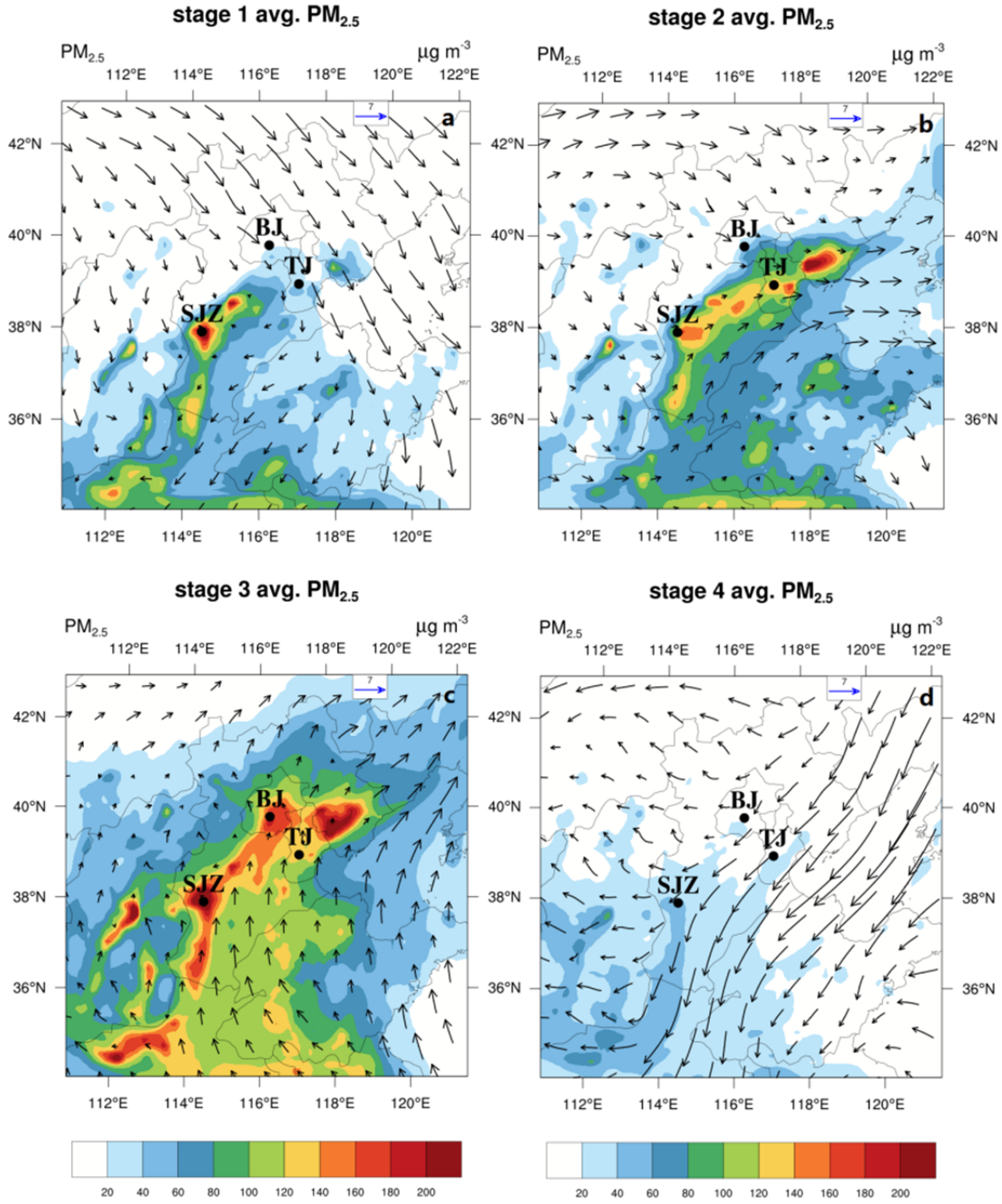

Fig. 5. a-d) Average spatial distribution of surface $PM_{2.5}$ and wind fields during four stages.

path so that they accumulated at the foot of the mountain. $PM_{2.5}$ pollution spread nearly the height of 3 km because of this special terrain and the southerly wind. The height of temperature inversion and PBLH near 200 m existed on the region of BJ and TJ. Fig. 9(b) (from the black southwest-northeast straight line in Fig. 8, including SJZ and the midpoint between TJ and BJ) shows that SJZ, BJ, and TJ lie in a large valley. And Pollutants were transported to the valley by the southerly wind and did not spread out easily because of the terrain. There is also a temperature inversion and a low PBLH in this valley. The height of the $PM_{2.5}$ pollution in the BTH region is higher than the other regions.

In general, a PBLH near 200 m with a temperature inversion was not conducive to the vertical diffusion of pollutants, which also further aggravated surface pollution levels in the BTH region. However, the BTH region is surrounded on three sides by tall mountains, which lead to vertical airflow. Therefore, the pollutants transported by the southerly wind were unable to spread horizontally, forced them to extend nearly 3 km upraised by terrain.

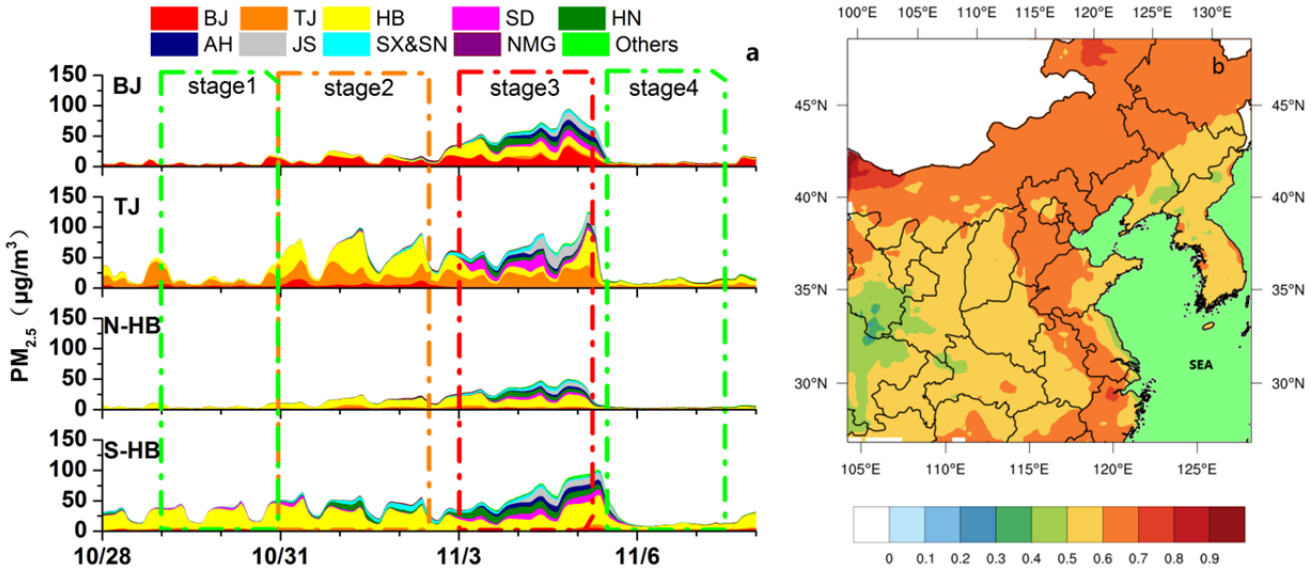

Fig. 6. a) Primary $PM_{2.5}$ contributions of different geographical source regions to the BTH region (including N-HB and S-HB), b) average spatial distribution of the primary-to-total $PM_{2.5}$ ratio.

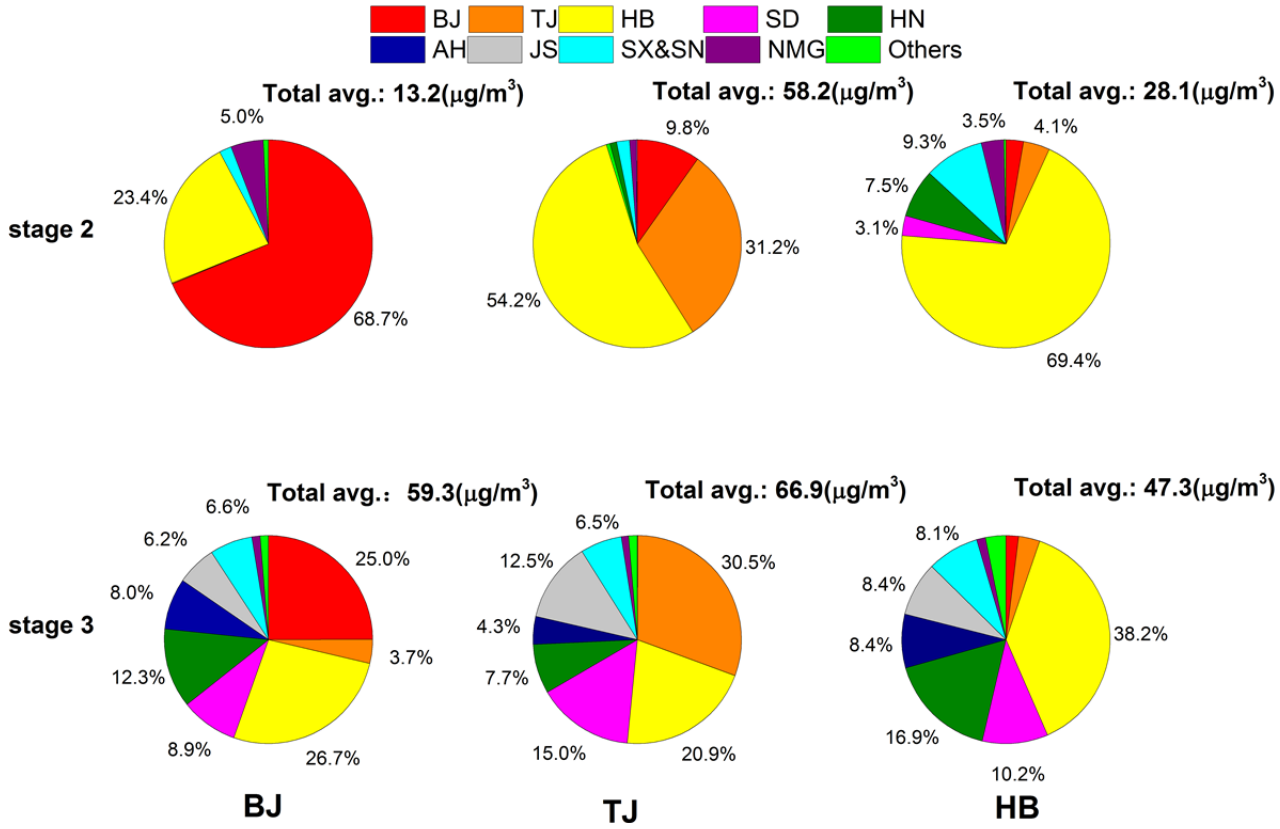

Fig. 7. Average primary $PM_{2.5}$ contributions by different geographical source regions to the BTH region during stages 2 and 3.

Long-Distance Transport Implicated by Primary $PM_{2.5}$ Tagging

Using the tagging method, Fig. 10 shows the distributions of average primary $PM_{2.5}$ contributions by four major source regions (JS, AH, HN, and SD) in stages 3a (on November 3) and 3b (from November 4 to 06:00 LST on November 5). In stage 3a (Figs. 10(a)–10(d)), JS, AH, HN and SD were behind high-pressure conditions, so this four source regions were controlled by the southerly wind. There was almost no contribution from JS on BTH, although the primary $PM_{2.5}$ concentration in JS reached about 100 μg m^{-3}. AH only exerted slight influence on S-HB. HN and SD are near BTH,

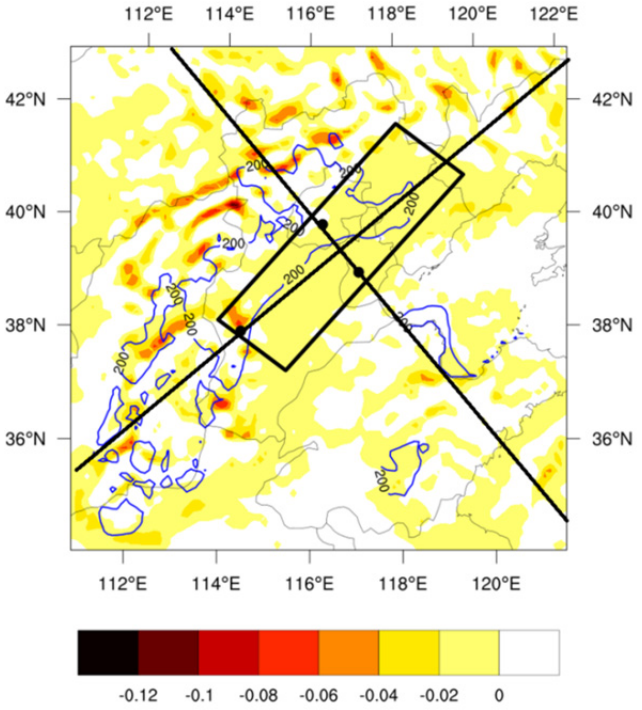

Fig. 8. Distribution of average PBLH and wind divergence in stage 3 (blue contours: boundary layer height of 200 m, black straight line: the positions of two vertical profiles used in Fig. 9, yellow shaded: horizontal distribution of wind divergence).

so pollutants from HN and SD were therefore transported to BTH more easily than from JS and AH. Therefore, HN affected the whole BTH region, and SD mainly affected TJ and S-HB via the southerly wind.

As high-pressure conditions moved east (stage 3b, Figs. 10(e)–10(h)), the site of gale also moved east so that JS experienced a southeast gale. JS significantly contributed pollutants to BTH, especially in southeastern HB and TJ. The primary $PM_{2.5}$ from AH and SD almost covered the entire BTH region. The wind speed in HN decreased after high-pressure conditions moved east, but HN continued to contribute pollutants to the BTH region. SD has a significantly contribution to the most BTH region.

Fig. 11 presents the average primary $PM_{2.5}$ contributions by different source regions in stages 3a and 3b. In stage 3a, primary $PM_{2.5}$ concentrations in the BTH region mainly originated locally and from HN, SX&SN. SD only contributed greatly to the TJ region (average primary $PM_{2.5}$ concentration 9.3 μg m^{-3}, accounting for 18.3%), while HN contributed significantly to the BTH region throughout stage 3a. During this period, JS exerted almost no effect on BTH. In stage 3b, the contributions in most significant source regions were greater than stage 3a, although the direct line distance from JS to BTH is about 850 km, but JS had a significant impact on BTH, especially in TJ, where the mean value reached 14.5 μg m^{-3} (accouting for 18.3%). The contributions by SD, HN, AH, and JS to S-HB were nearly twice those to N-HB during stage 3b, thus, the major polluted area in HB was S-HB.

In conclusion, under the influence of a high-pressure system, the JS, AH, HN and SD region contributed significant levels of primary $PM_{2.5}$ to the BTH region via the southerly wind. So a source in the Yangtze River Delta city group region played a significant role in the BTH region. Although JS only affected the BTH region about one day, its primary $PM_{2.5}$ contribution could not be ignored. The higher primary $PM_{2.5}$ concentration in HB illustrated that HB, especially S-HB, played a key role in high primary $PM_{2.5}$ events over the BTH region.

CONCLUSION

In this study, the WRF-Chem model coupled with an online primary aerosol tagging method was used to simulate

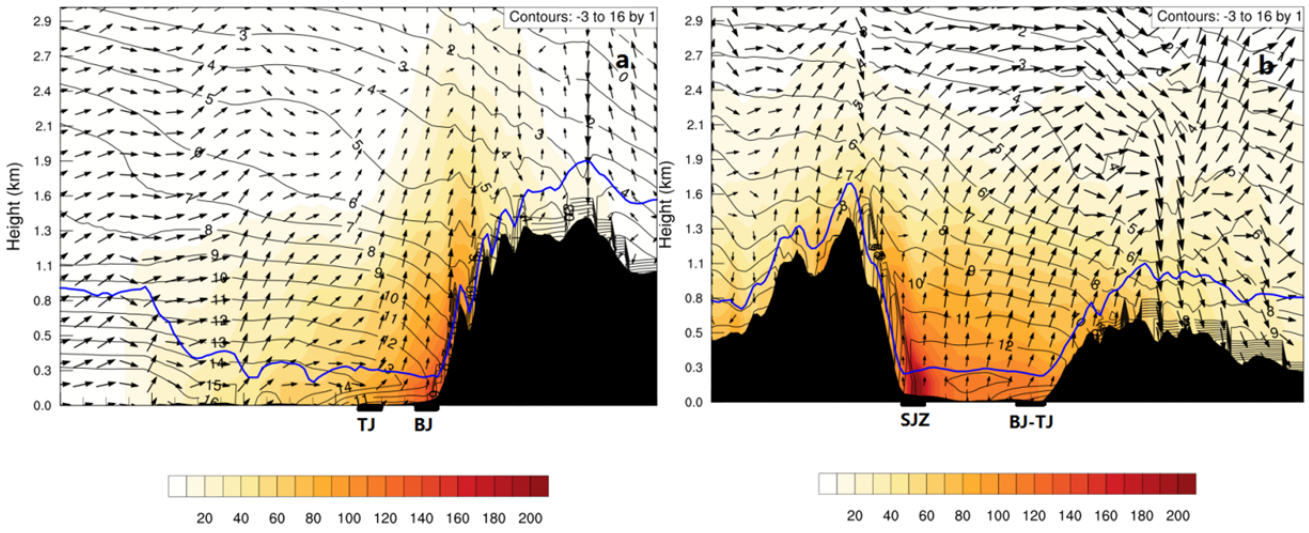

Fig. 9. a) Vertical profile of temperature and $PM_{2.5}$ concentration with southeast-northwest boundary layer height, b) vertical profile of temperature and $PM_{2.5}$ concentration with southwest-northeast boundary layer height (black line: isotherm, blue line: boundary layer height, black areas: terrain , and the vertical wind was enlarged 200 times).

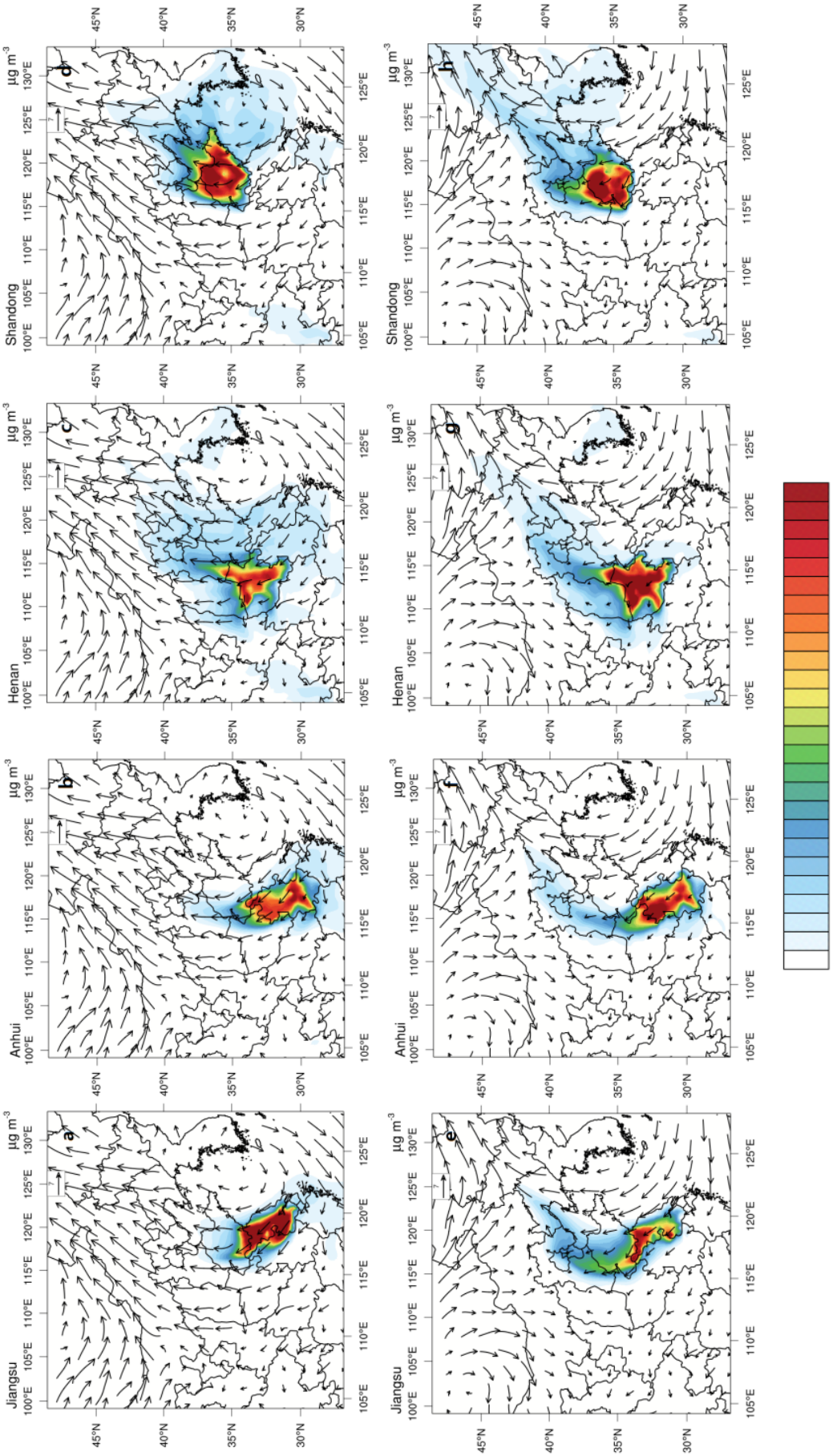

Fig. 10. Spatial distribution of average primary $PM_{2.5}$ contributions by four major source regions during stage 3a: a) JS, b) AH, c) and HN, d) SD and stage 3b: e) JS, f) AH, g) HN, and h) SD.

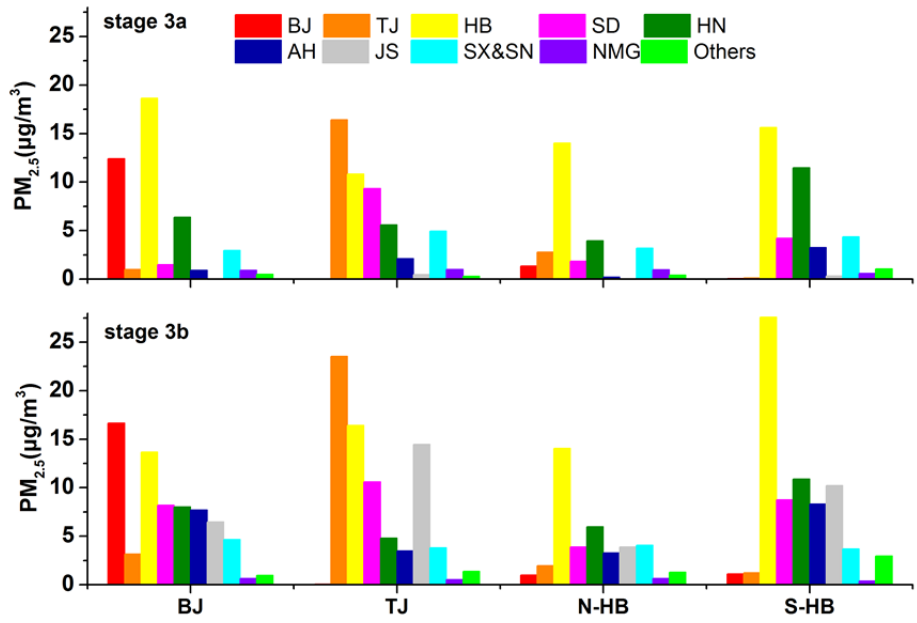

Fig. 11. Contributions of average primary $PM_{2.5}$ by different source regions to BJ, TJ, and HB (S-HB and N-HB) in stages 3a and 3b.

an episode of high concentration of $PM_{2.5}$ that occurred in the BTH region in late October and early November 2015. The primary $PM_{2.5}$ contributions by different geographical source regions to the BTH region were quantified. Using the model, we evaluated both meteorological variables and $PM_{2.5}$ concentrations with confidence, and our conclusions are summarized below.

The simulation showed that pollution in the BTH region was mainly affected by synoptic conditions, the terrain, and boundary layer characteristics. The distribution and concentrations of pollutants differed under various surface synoptic conditions, with pollution primarily originating locally from October 29 to 30, locally and in surrounding areas from October 31 to 12:00 LST on November 2, and in a wide geographic area (and brought to the BTH region via long-distance transport) from November 3 to 06:00 LST on November 5.

The clear contribution and spatial distribution of average primary $PM_{2.5}$ from different geographical source regions showed the trajectory of primary $PM_{2.5}$ transported to the BTH region. To a certain extent, the primary $PM_{2.5}$ with a high percentage within total $PM_{2.5}$ can represent the characteristics of total $PM_{2.5}$. The primary $PM_{2.5}$ source appointment results clearly presented that before the heavy pollution event, the BTH region was mainly originated locally accounted for 90.7% of the total primary $PM_{2.5}$. When the BTH region was under isobaric synoptic condition and the pollution was most serious throughout the four stages, contributed by locally and other polluted areas, especially SD, HN, AH, and JS, with average primary $PM_{2.5}$ contributions of 50.7%, 11.6%, 11.8%, 6.7% and 9.2%, respectively. Primary $PM_{2.5}$ from local (the BTH region) and non-local regions contributed nearly equally during the heavy pollution. These accurate contribution results showed that the BTH region was affected by not only the locally and the surrounding cities but also the areas from the regional scale or even larger.

Vertically, during periods of heavy pollution, a PBLH near 200 m with a temperature inversion and the terrain of the BTH region surrounded on three sides by tall mountains were not conducive to the vertical and horizontal diffusion of pollutants. However, the vertical airflow caused by the terrain forced the pollutants to upraise and extend nearly 3 km via the southerly wind.

ACKNOWLEDGMENTS

This work is supported by grants from the National Natural Science Foundation of China (Grant No. 91544229), the National Key Research and Development Program of China (2016YFA0602003). The observational data of $PM_{2.5}$ concentrations are available at http://106.37.208.233:20035, and the observational meteorological data are obtained from Meteorological Information Comprehensive Analysis and Process System (MICAPS). Weather maps are obtained from Korea Meteorological Administration (KMA). Please email us via binzhu@nuist.edu.cn or ylzhang219@126.com if you have any question.

SUPPLEMENTARY MATERIAL

Supplementary data associated with this article can be found in the online version at http://www.aaqr.org.

REFERENCES

An, X.Q., Zhu, T., Wang, Z.F., Li, C.Y. and Wang, Y.S. (2007). A modeling analysis of a heavy air pollution episode occurred in Beijing. *Atmos. Chem. Phys.* 7: 3103–3114.

Brook, R.D. and Rajagopanlan, S. (2010). Particulate matter

air pollution and atherosclerosis. *Curr. Atherosclerosis Rep*. 12: 291–300.

Chen, F. and Dudhia, J. (2001). Coupling an advanced land surface-hydrology model with the Penn State-NCAR MM5 modeling system. Part I: Model implementation and sensitivity. *Mon. Weather Rev.* 129: 569–585.

Chou, M.D. and Suarez, M.J. (1994). An efficient thermal infrared radiation parameterization for use in general circulation models. NASA Technical Memorandum, 104606 Vol. 3.

Ding, A.J., Fu, C.B., Yang, X.Q., Sun, J.N., Petäjä, T., Kerminen, V.M., Wang, T., Xie, Y., Herrmann, E., Zheng, L.F., Nie, W., Liu, Q., Wei, X.L. and Kulmala, M. (2013). Intense atmospheric pollution modifies weather: A case of mixed biomass burning with fossil fuel combustion pollution in eastern China. *Atmos. Chem. Phys.* 13: 10545–10554.

Fan, S.X., Xu, J.Q., Zheng, Y.F. and Xie, X.J. (2005). A sources apportionment of aerosols $PM_{2.5}$ over the urban and suburb areas of Nanjing. *Sci. Meteorol. Sin*. 25: 587–593 (in Chinese).

Gao, J.H., Zhu, B., Xiao, H., Kang, H.Q., Hou, X.W. and Shao, P. (2016). A case study of surface ozone source apportionment during a high concentration episode under frequent shifting wind conditions over the Yangtze River Delta, China. *Sci. Total Environ*. 544: 853–863.

Grell, G.A. (1993). Prognostic evaluation of assumptions used by cumulus parameterizations. *Mon. Weather Rev*. 121: 764–787.

Grell, G.A., Peckham, S.E., Schmitz, R., McKeen, S.A., Frost, G., Skamarock, W.C. and Eder, B. (2005). Fully coupled "online" chemistry within the WRF model. *Atmos. Environ*. 39: 6957–6975.

Guo, L., Zang, Y., Liu, S., Li, J. and Ma, Y. (2011). Correlation analysis between PM_{10} Mass concentration and meteorological elements of atmospheric boundary layer in Beijing area. *Acta Sci. Nat. Univ. Pekin*. 47: 607–612.

He, K.B., Yang, F.M., Duan, F.K. and Ma, Y.L. (2011). *Atmospheric Particulates and Regional Complex Air Pollution*. Beijing: Science Press, (in Chinese).

Hong, S.Y., Noh, Y. and Dudhia, J. (2006). A new vertical diffusion package with an explicit treatment of entrainment processes. *Mon. Weather Rev*. 134: 2318–2341.

Huang, Q., Cheng, S., Li, J., Chen, D., Wang, H. and Guo, X. (2012). Assessment of PM_{10} emission sources for priority regulation in urban air quality management using a new coupled MM5-CAMx-PSAT modeling approach. *Environ. Eng. Sci*. 29: 343–349.

Huang, R.J., Zhang, Y., Bozzetti, C., Ho, K.F., Cao, J.J., Han, Y., Daellenbach, K.R., Slowik, J.G., Platt, S.M., Canonaco, F., Zotter, P., Wolf, R., Pieber, S.M., Bruns, E.A., Crippa, M., Ciarelli, G., Piazzalunga, A., Schwikowski, M., Abbaszade, G., Schnelle-Kreis, J., Zimmermann, R., An, Z., Szidat, S., Baltensperger, U., El Haddad, I. and Prévôt, A.S. (2014). High secondary aerosol contribution to particulate pollution during haze events in China, *Nature* 514: 218–222.

Ji, D.S., Wang, Y.S., Wang, L.L., Chen, L.F., Hu, B., Tang, G.Q., Xin, J.Y., Song, T., Wen, T.X., Sun, Y., Pan, Y.P. and Liu, Z.R. (2012). Analysis of heavy pollution episodes in selected cities of northern China. *Atmos. Environ*. 50: 338–348.

Li, C., Huo, S., Yu, Z., Xi, B., Zeng, X. and Wu, F. (2014). Spatial distribution, potential risk assessment, and source apportionment of polycyclic aromatic hydrocarbons (PAHs) in sediments of Lake Chaohu, China. *Environ. Sci. Pollut. Res. Int.* 21: 12028–12039.

Li, J., Wang, Z., Akimoto, H., Yamaji, K., Takigawa, M., Pochanart, P., Liu, Y., Tanimoto, H. and Kanaya, Y. (2008). Near-ground ozone source attributions and outflow in central eastern China during MTX2006. *Atmos. Chem. Phys*. 8: 7335–7351.

Lin, Y.L., Farley, R.D. and Orville, H.D. (1983). Bulk parameterization of the snow field in a cloud model. *J. Clim. Appl. Meteorol*. 22: 1065–1092.

Liu, S.X., An, J.L. and Zhu, B. (2010). Influence of the long-distance air masses on atmospheric pollutants in Nanjing city. *Ecol. Environ.* 11: 2629–2635 (in Chinese).

Liu, T., Huang, X.Y., Gao, Q.X., Zhan-Yun, M.A. and Xie, B. (2013). Research on the temporal and spatial distribution of atmospheric aerosols under different meteorological conditions. *Res. Environ. Sci*. 26: 122–128 (in Chinese).

Lyu, Y., Jaeger, C., Han, Z., Liu, L., Shi, P., Wang, W., Yang, S., Guo, L., Zhang, G., Hu, X., Guo, J., Gao, Y., Yang, Y., Xiong, Y., Wen, H., Liang, B. and Zhao, M. (2015). A Severe air pollution event from field burning of agricultural residues in Beijing, China. *Aerosol Air Qual. Res*. 15: 2525–2536.

Meng, Y.J. and Cheng, C.L. (2002). Impact of surface synoptic situations on air pollution in Beijing Area. *Meteorol. Mon.* 4: 42–47 (in Chinese).

Miao, Y.C., Zheng, Y.J., Wang, S. and Liu, S.H. (2015). Recent advances in, and future prospects of, research on haze formation over Beijing-Tianjin-Hebei, China. *Clim. Environ. Res.* 20: 356–368 (in Chinese).

Mlawer, E.J., Taubman, S.J., Brown, P.D., Iacono, M.J. and Clough, S.A. (1997). Radiative transfer for inhomogeneous atmospheres: RRTM, a validated correlated-k model for the longwave. *J. Geophys. Res*. 102: 16663–16682.

Okajima, S., Matsuda, T., Cho, K., Matsumoto, Y., Kobayashi, Y. and Fujimoto, S. (2001). Antenatal dexamethasone administration impairs normal postnatal lung growth in rats. *Pediatr. Res*. 49: 777–781.

Parrish, D.D. and Zhu, T. (2009). Clean air for megacities. *Science* 326: 674–675.

Perry, K.D., Cahill, T.A., Eldred, R.A., Dutcher, D.D. and Gill, T.E. (1997). Long-range transport of north African dust to the eastern United States. *J. Geophys. Res*. 102: 11225–11238.

Pope, C.A., Burnett, R.T., Thurston, G.D., Thun, M.J., Calle, E.E., Krewski, D. and Godleski, J.J. (2004). Cardiovascular mortality and long-term exposure to particulate air pollution: Epidemiological evidence of general pathophysiological pathways of disease. *Circulation (Baltimore)* 109: 71–77.

Ren, Z.H., Wan, B.T., Yu, T., Su, F.Q., Zhang, Z.G., Gao, Q.X., Yang, X.X., Hu, H.L., Wu, Y.H., Hu, F. and Hong,

Z.X. (2004). Influence of weather system of different scales on pollution boundary layer and the transport in horizontal current field. *Res. Environ. Sci.* 17: 7–13 (in Chinese).

Skamarock, W.C., Klemp, J.B., Dudhia, J., Gill, D.O., Barker, D.M., Wang, W. and Powers, J.G. (2005). A description of the advanced research WRF version 2. NCAR Technical Note. NCAR/TN/u2013475.

Streets, D.G., Fu, J.S., Jang, C.J., Hao, J., He, K., Tang, X., Zhang, Y., Wang, Z., Li, Z., Zhang, Q., Wang, L., Wang, B. and Yu, C. (2007). Air quality during the 2008 Beijing Olympic Games. *Atmos. Environ*. 41: 480–492.

Wagstrom, K.M., Pandis, S.N., Yarwood, G., Wilson, G.M. and Morris, R.E. (2008). Development and application of a computationally efficient particulate matter apportionment algorithm in a three-dimensional chemical transport model. *Atmos. Environ*. 42: 5650–5659.

Wang, F., Zhu, B., Kang, H.Q., Gao, J.H., Wang, Y. and Jiang, Q. (2012). Analysis of the impact of two typical air pollution events on the air quality of Nanjing. *Environ. Sci*. 10: 3647–3655 (in Chinese).

Wang, Y., Chai, F.H., Wang, Y.H. and Liu, M. (2008). Transport characteristics of air pollutants over the Yangtze Delta. *Environ. Sci.* 5: 1430–1435 (in Chinese).

Wang, Y.S., Li, Y., Wang, L.L., Liu, Z.R., Ji, D.S., Tang, G.Q., Zhang, J.K., Sun, Y., Hu, B. and Xin, J.Y. (2014). Mechanism for the formation of the January 2013 heavy haze pollution episode over central and eastern China. *Sci. China Earth Sci.* 57: 14–25 (in Chinese).

Wang, Z.F., Li, J., Wang, Z., Yang, W.Y., Tang, X., Ge, B.Z., Yan, P.Z., Zhu, L.L., Chen, X.S., Chen, H.S., Wang, W., Li, J.J., Liu, B., Wang, X.Y., Wang, W., Zhao, Y.L., Lu, N. and Su, D.B. (2014). Modeling study of regional severe hazes over Mid-Eastern China in January 2013 and its implications on pollution prevention and control. *Sci. China Earth Sci.* 57: 3–13 (in Chinese).

Wesely, M.L. (1989). Parameterization of surface resistances to gaseous dry deposition in regional-scale numerical models. *Atmos. Environ.* 23: 1293–1304.

Wild, O., Zhu, X. and Prather, M.J. (2000). Fast-J: Accurate simulation of in-and below-cloud photolysis in tropospheric chemical models. *J. Atmos. Chem*. 37: 245–282.

Wu, D., Liao, B.T., Wu, M., Chen, H.Z., Wang, Y.C., Liao, X.N., Gu, Y., Zhang, X.L., Zhao, X.J., Quan, J.N., Liu, W.D., Meng, J.P. and Sun, D. (2014). The long-term trend of haze and fog days and the surface layer transport conditions under haze weather in North China. *Acta Sci. Circumst.* 34: 1–11 (in Chinese).

Wu, Q.Z., Wang, Z.F., Gbaguidi, A., Gao, C., Li, L.N. and Wang, W. (2011). A numerical study of contributions to air pollution in Beijing during CARE Beijing-2006. *Atmos. Chem. Phys*. 11: 5997–6011.

Yang, J., Li, X., Li, Q. and Wang, Z.W. (2011). Variation characteristics of atmospheric stability and mixed layer thickness and their relation to air pollution in recent 30 years in Urumqi. *Arid Land Geogr*. 34: 747–752.

Yang, P., Zhu, B., Gao, J.H., Kang, H.Q., Zhang, L., Wang, H.L. and Li, Y.E. (2016). A numerical simulate study of the pollution incident of the $PM_{2.5}$ pollutant island in the summer of Nanjing. *China Environ. Sci.* 2: 321–330 (in Chinese).

Ye, D., Wang, F. and Chen, D. (2008). Multi-year changes of atmospheric mixed layer thickness and its effect on air quality above Chongqing. *Meteorol. Environ.* 24: 41–44 (in Chinese).

Ying, Q. and Kleeman, M.J. (2006). Source contributions to the regional distribution of secondary particulate matter in California. *Atmos. Environ*. 40: 736–752.

Zaveri, R.A. and Peters, L.K. (1999). A new lumped structure photochemical mechanism for large-scale applications. *J. Geophys. Res*. 104: 30387–30415.

Zaveri, R.A., Easter, R.C., Fast, J.D. and Peters, L.K. (2008). Model for simulating aerosol interactions and Chemistry (MOSAIC). *J. Geophys. Res*. 113: D13204.

Zhang, R., Wang, G., Guo, S., Zamora, M.L., Ying, Q., Lin, Y., Wang, W., Hu, M. and Wang, Y. (2015). Formation of urban fine particulate matter. *Chem. Rev*. 115: 3803–3855.

Zhang, X.Y., Sun, J.Y., Wang, Y.Q., Li, W.J., Zhang, Q., Wang, W.G., Quan, J.N., Cao, G.L., Wang, J.Z., Yang, Y.Q. and Zhang, Y.M. (2013). Factors contributing to haze and fog in China. *Chinese Sci. Bull.* 58: 1178–1187 (in Chinese).

Zhao, X., Zhang, X., Xu, X., Xu, J., Meng, W. and Pu, W. (2009). Seasonal and diurnal variations of ambient $PM_{2.5}$ concentration in urban and rural environments in Beijing. *Atmos. Environ.* 43: 2893–2900.

Received for review, October 13, 2016
Revised, March 2, 2017
Accepted, April 16, 2017